Received: 17 January 2021 | Revised: 26 June 2021 | Accepted: 29 June 2021

DOI: 10.1002/mrc.5188

SPECIAL ISSUE RESEARCH ARTICLE

WILEY

^{35}Cl–^{1}H Heteronuclear correlation magic-angle spinning nuclear magnetic resonance experiments for probing pharmaceutical salts

Dinu Iuga | **Emily K. Corlett** | **Steven P. Brown**

Department of Physics, University of Warwick, Coventry, UK

Correspondence
Dinu Iuga, Department of Physics, University of Warwick, Coventry CV4 7AL, UK.
Email: d.iuga@warwick.ac.uk.

Funding information
Engineering and Physical Sciences Research Council (EPSRC), Grant/Award Number: EP/L015307/1; Biotechnology and Biological Sciences Research Council (BBSRC), Grant/Award Numbers: PR140003, EP/T015063/1

Abstract

Heteronuclear multiple-quantum coherence (HMQC) pulse sequences for establishing heteronuclear correlation in solid-state nuclear magnetic resonance (NMR) between ^{35}Cl and ^{1}H nuclei in chloride salts under fast (60 kHz) magic-angle spinning (MAS) and at high magnetic field (a ^{1}H Larmor frequency of 850 MHz) are investigated. Specifically, recoupling of the ^{35}Cl–^{1}H dipolar interaction using rotary resonance recoupling with phase inversion every rotor period or the symmetry-based SR4$^{2}_{1}$ pulse sequences are compared. In our implementation of the population transfer (PT) dipolar (D) HMQC experiment, the satellite transitions of the ^{35}Cl nuclei are saturated with an off-resonance WURST sweep, at a low nutation frequency, over the second spinning sideband, whereby the WURST pulse must be of the same duration as the recoupling time. Numerical simulations of the ^{35}Cl–^{1}H MAS D-HMQC experiment performed separately for each crystallite orientation in a powder provide insight into the orientation dependence of changes in the second-order quadrupolar-broadened ^{35}Cl MAS NMR lineshape under the application of dipolar recoupling. Two-dimensional ^{35}Cl–^{1}H PT-D-HMQC MAS NMR spectra are presented for the amino acids glycine·HCl and L-tyrosine·HCl and the pharmaceuticals cimetidine·HCl, amitriptyline·HCl and lidocaine·HCl·H_2O. Experimentally observed ^{35}Cl lineshapes are compared with those simulated for ^{35}Cl chemical shift and quadrupolar parameters as calculated using the gauge-including projector-augmented wave (GIPAW) method: the calculated quadrupolar product (P_Q) values exceed those measured experimentally by a factor of between 1.3 and 1.9.

1 | INTRODUCTION

Chloride salts have wide application in the isolation and purification of active pharmaceutical ingredients (APIs). The use of salts provides higher concentration in solution, and they readily undergo crystallisation. Another advantage for using salts is that they provide more stability as preservatives, acting as an antimicrobial component designed to destroy or inhibit the growth of bacteria, yeast or moulds and extend the shelf life of

medicine.[1] Last but not least the use of salts increases the bioavailability of the APIs by increasing their solubility and/or enhancing their permeability across membranes.[2] The relevance of chlorine when preparing pharmaceuticals is evident considering that a large proportion (up to about 50%) of APIs are formulated as HCl salts.[3] Introduction of a chloride ion is associated with protonation of a specific site in the API so as to achieve charge balance; this usually affects the position of the hydrogen atoms, affecting the intermolecular interactions, the supramolecular assembly and thus the solubility, stability, bioavailability and biological activity[4]; therefore, high-resolution structural characterisation of the API and polymorph identification[5] is required.

As well as complementary ^{1}H, ^{13}C, $^{14/15}$N solid-state NMR experiments,[6] it is clearly beneficial to directly probe the chlorine nuclei. The ^{35}Cl nucleus has 75% natural abundance and is a quadrupolar nucleus, with a nuclear spin $I = 3/2$. The quadrupolar interaction provides information about symmetry and the local environment of such nuclei, therefore contributing to the structural characterization endeavour with complementary information, hence the continuous effort to develop NMR methodology to obtain structural information from ^{35}Cl NMR.[7–11] In many organic compounds where it is covalently bound, the ^{35}Cl nucleus experiences a very large quadrupolar interaction not amenable to MAS experiments.[12] However, in hydrochloride salts of, for example, amino acids and pharmaceuticals, the chloride ions are ionically bonded; therefore, the quadrupolar interaction is reduced due to increased symmetry, and the ^{35}Cl MAS NMR signal can be measured at high magnetic fields and/or under very fast MAS.[5,13–18]

When dealing with half-integer quadrupolar nuclei, it is usually beneficial to saturate the satellite transitions and thus increase the polarisation of the central transition before the 90° excitation pulse.[19–23] This can be achieved using a fast 180° phase alternating pulse train that induces rotor-assisted population transfer (RAPT),[19] or a double frequency sweep (DFS) achieved by a time dependent amplitude modulated pulse that sweeps over the satellite transitions,[20] or a hyperbolic secant π inversion pulse,[21,24] or a WURST shaped pulse,[22] or repetitive sideband-selective DFS,[25,26] or using quadruple frequency sweeps.[27] An analysis of all orientations in a powder shows that such saturation can be uniformly achieved over all different orientations for the quadrupolar interaction in a powder, and therefore, no significant lineshape distortion is expected.[20] In this work, we are using an off-resonance WURST pulse sweeping over a spinning sideband, which provides a good saturation of the satellite transition and a significant signal enhancement in the ^{35}Cl MAS NMR spectra.

Accurate localization of chloride ions in pharmaceutical salts is important for structural characterization. In this context, it is possible to measure internuclear distances between ^{35}Cl and ^{13}C nuclei using a REAPDOR experiment as was demonstrated for 10% ^{13}C-enriched tyrosine·HCl and natural abundance glycine·HCl.[28] Proximities between ^{13}C and ^{35}Cl in histidine HCl monohydrate have also been probed using a DNP-enhanced D-HMQC experiment.[7] Further structural information can be obtained by investigating proximities between Cl and H atoms. With advances in fast MAS technology, involving the ^{1}H nucleus in solid-state NMR experiments becomes advantageous. Under fast MAS, not only the resolution in the ^{1}H MAS NMR spectra is enhanced, but also the spin-echo lifetimes become considerably longer opening up the possibility to investigate ^{1}H environments by recoupling the heteronuclear dipolar coupling between protons and another adjacent NMR active nucleus such as ^{14}N, ^{17}O or ^{35}Cl.[29–32] Here, we consider rotary resonance recoupling[33] with the RF phase inverted every rotor period[34] and symmetry-based recoupling[35–37] of the ^{35}Cl–^{1}H dipolar coupling.

For two-dimensional (2D) heteronuclear experiments considered in this paper, the nuclei are specified in the order of, first, the indirect and, second, the direct dimension, that is, F_1–F_2. The ^{14}N–^{1}H dipolar HMQC (D-HMQC) MAS experiment[38–40] has been successfully used to detect nitrogen–hydrogen proximities,[29] for example, to identify specific intermolecular hydrogen bonding interactions in an indomethacin–nicotinamide co-crystal,[41] a nicotinamide palmitic acid co-crystal and an acetaminophen–polyvinylpyrrolidone solid dispersion,[42] or to probe nitrogen protonation in cimetidine.[43] The spin dynamics of quadrupolar nuclei under the HMQC experiment has been recently described.[44,45] Specifically, Wang et al.[44] introduced the population transfer (PT)-D-HMQC experiment to probe ^{27}Al–^{31}P correlations where the satellite transitions of the ^{27}Al are saturated with a WURST irradiation during symmetry-based recoupling. In addition, frequency selective HMQC or RESPDOR[46,47] experiments that have been implemented for ^{14}N–^{1}H can also be applied in ^{35}Cl–^{1}H applications. Venkatesh et al. have presented a ^{35}Cl–^{1}H D-HMQC experiment that incorporates saturation of the satellite transitions using RAPT during the mixing time.[31] Venkatesh et al. have also investigated an alternative experiment, D-RINEPT, to obtain ^{35}Cl–^{1}H correlations. In this paper, we explore the applicability of the ^{35}Cl–^{1}H PT-D-HMQC experiment to probe proximities between hydrogen and chlorine atoms in the amino acids glycine·HCl and L-tyrosine·HCl and the pharmaceuticals cimetidine·HCl, amitriptyline·HCl and lidocaine·HCl·H_2O.

2 | EXPERIMENTAL AND COMPUTATIONAL DETAILS

L-Tyrosine·HCl, glycine·HCl, lidocaine·HCl·H_2O, cimetidine·HCl and amitriptyline·HCl were purchased from Sigma-Aldrich and used without further purification. Experiments were performed on a Bruker Avance Neo spectrometer with a Larmor frequency of 850.2 and 83.3 MHz for ^{1}H and ^{35}Cl, respectively, using a 1.3-mm Bruker triple-resonance HXY probe operating in double-resonance mode at 60 kHz MAS. The ^{35}Cl NMR spectra were referenced to a NaCl 0.1-M aqueous solution with the ^{35}Cl peak set to 0 ppm.[13] To convert to a chemical shift scale where the ^{35}Cl of solid NaCl is set to 0 ppm, it is necessary to add 46.34 ppm (Eq. 6 in Bryce et al.[13]). The ^{1}H NMR spectra were referenced to the ^{1}H peak of adamantane set to 1.8 ppm.[32,48,49] A ^{1}H nutation frequency of 140 kHz was used for ^{1}H 90° and 180° pulses. ^{1}H one-pulse MAS NMR spectra were measured using the standard Bruker background suppression pulse sequence consisting of a 180° pulse followed by two 90° pulses.[50] The same recycle delay of 1 s was used for each sample, though it may be possible to optimise sensitivity by optimising the recycle delay to the sample's specific ^{1}H T_1 value.

Phase-inverted (i.e., *x*–*x* phase inversion each rotor period) R^{3}[33,34,51,52] or $SR4^{2}_{1}$[35–37,40] heteronuclear recoupling was applied on the ^{1}H channel at a nutation frequency of 120 kHz. WURST[22,23,53,54] saturation pulses at 5 kHz (central transition) nutation frequency were applied on the ^{35}Cl channel during the recoupling. In our implementation for the ^{35}Cl experiments in this paper, the WURST pulses are centred at an offset of 120 kHz, that is, the second spinning sideband and sweep over 40 kHz from low to high ppm. We observe that the success of the ^{35}Cl–^{1}H experiment requires the duration of the WURST saturation pulses to be the same as the duration of the $SR4^{2}_{1}$ recoupling as has previously been applied by Wang et al.[44] in a PT-D-HMQC ^{27}Al–^{31}P experiment.[45] The ^{35}Cl central transition was excited with a 2.1-μs pulse at a central transition nutation frequency of 120 kHz. The 2D D-HMQC spectra were acquired using States phase incrementation in the t_1 dimension.[55] ^{35}Cl MAS spectra were measured using the standard Bruker spin-echo pulse sequence preceded by a WURST saturation.

First-principle calculations were performed using the academic release version 16.1 of CASTEP,[56] using the Perdew–Burke–Ernzerhof (PBE) exchange correlation functional,[57] a plane-wave basis set with ultrasoft pseudopotentials and a plane-wave cut-off energy of 700 eV. Geometry optimization was performed starting with the respective X-ray structure as deposited at the Cambridge Structural Database. NMR parameters were calculated using the gauge-including projector-augmented wave (GIPAW)[58] method with a reference chemical shielding of 30 and 962 ppm for ^{1}H and ^{35}Cl, respectively.

3 | RESULTS AND DISCUSSION

3.1 | Evaluation of ^{35}Cl–^{1}H D-HMQC MAS NMR pulse sequences

The ^{35}Cl–^{1}H D-HMQC solid-state NMR pulse sequences employed in this work are shown in Figure 1. $SR4^{2}_{1}$[35–37,40] or phase-inverted R^{3}[33,34,51,52] recoupling is applied on the ^{1}H channel to recouple the ^{35}Cl–^{1}H heteronuclear dipolar coupling. Note that, in both cases, the nutation frequency is set to be twice the spinning frequency such that the ^{35}Cl–^{1}H heteronuclear dipolar interaction is reintroduced, while removing the ^{1}H–^{1}H homonuclear dipolar interaction. On the ^{35}Cl channel, a WURST saturation pulse[22,23,53,54] sweeping over the

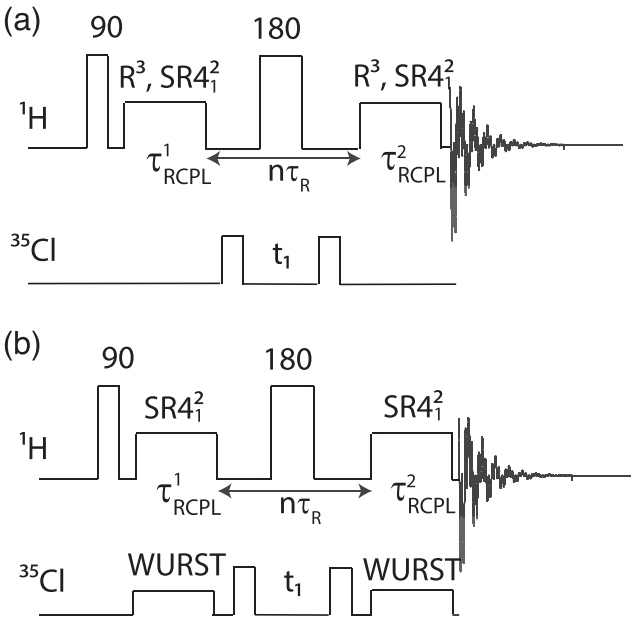

FIGURE 1 Pulse sequences for a ^{35}Cl–^{1}H dipolar heteronuclear multiple-quantum coherence (D-HMQC) magic-angle spinning (MAS) nuclear magnetic resonance (NMR) experiment (a) without or (b) with a WURST saturation pulse applied to ^{35}Cl. Phase-inverted R^{3} or $SR4^{2}_{1}$ is employed to recouple the ^{35}Cl–^{1}H dipolar interaction. The simultaneous application of satellite transition saturation, here using WURST, and heteronuclear recoupling is referred to as a population transfer (PT)-D-HMQC experiment.[44] The delays before and after the application of the first recoupling block and after the application of the second recoupling block are kept as short as possible

second spinning sideband (with MAS at 60 kHz, the WURST offset is set to 120 kHz) saturates the satellite transition of the ^{35}Cl and increases the polarisation of the central transition. The pulse sequence in Figure 1a with $SR4^2_1$ recoupling has been demonstrated by Pandey et al. on L-tyrosine·HCl, L-histidine·HCl·H_2O, procainamide·HCl and aminoguanidine·HCl.[30] Venkatesh et al. use a PT-D-HMQC pulse sequence similar to that shown in Figure 1b except that for saturation of the satellite transitions, they use RAPT,[19] whereas we found that at fast spinning frequency, a low-nutation frequency WURST shape pulse, sweeping a 40 kHz range over the second spinning side band, saturates the satellites transitions efficiently.

Figure 2 presents 2D ^{35}Cl–^{1}H D-HMQC MAS NMR spectra of L-tyrosine·HCl with $SR4^2_1$ heteronuclear recoupling recorded (a) without or (b) with the application of WURST saturation pulses to ^{35}Cl. Strong peaks are observed at ^{1}H chemical shifts of 9.7 and 7.3 ppm corresponding to the OH and NH_3^+ moieties, with weaker correlation peaks for the COOH at 12.2 ppm as well as the lower ppm aromatic CH and aliphatic CH and CH_2 groups. Whereas the spectrum without saturation pulses shows ^{1}H peaks coupled with the ^{35}Cl central transition and with the ^{35}Cl satellite transitions, as observed previously by Pandey et al.,[30] the spectrum obtained with the WURST saturation pulses applied to ^{35}Cl only shows ^{1}H peaks with the ^{35}Cl central transition. Venkatesh et al. have previously observed such a suppression of the satellite transition peak using RAPT.[31] In the case that the 90° pulses on ^{35}Cl are selective on the ^{35}Cl central transition, the signal from the ^{35}Cl satellite transitions would also be reduced.[31,59]

Figure 3 presents comparisons of summed rows from the 2D ^{35}Cl–^{1}H D-HMQC MAS NMR spectra of L-tyrosine·HCl. Specifically, Figure 3a corresponds to a sum over only the ^{35}Cl central transition peaks. The application of $SR4^2_1$ recoupling with ^{35}Cl WURST satellite transition saturation gives 1.8 and 2.2 times more signal for the OH and NH_3^+ peak, respectively. Similar gains have been reported for ^{35}Cl–^{1}H PT-D-HMQC MAS NMR spectra of L-histidine HCl.[31] This signal gain is due to transfer from the satellite transitions into the central transition: in Figure 3b, which corresponds to the sum over the satellite and central transitions, the signal intensity is very similar for $SR4^2_1$ recoupling with and without WURST satellite transition saturation. Note that for the same recoupling time, we observe greater signal intensity with $SR4^2_1$ as compared with phase-inverted R^3 recoupling. All subsequent ^{35}Cl–^{1}H D-HMQC MAS NMR spectra presented in the rest of this paper were recorded using the PT-D-HMQC pulse sequence in Figure 1b, that is, with $SR4^2_1$ recoupling and WURST saturation of the ^{35}Cl satellite transitions.

3.2 | Dependence on recoupling time and on quadrupolar orientation

This section explores the extent to which performing the PT-D-HMQC experiment with different recoupling times reveals quantitative information about ^{35}Cl–^{1}H distances. Figure 4a compares the signal intensity for the L-tyrosine·HCl ^{1}H resonances (the displayed ^{1}H spectral width is from 1.0 to 11.2 ppm) for different $SR4^2_1$ recoupling times at 60 kHz MAS. For this experiment, both

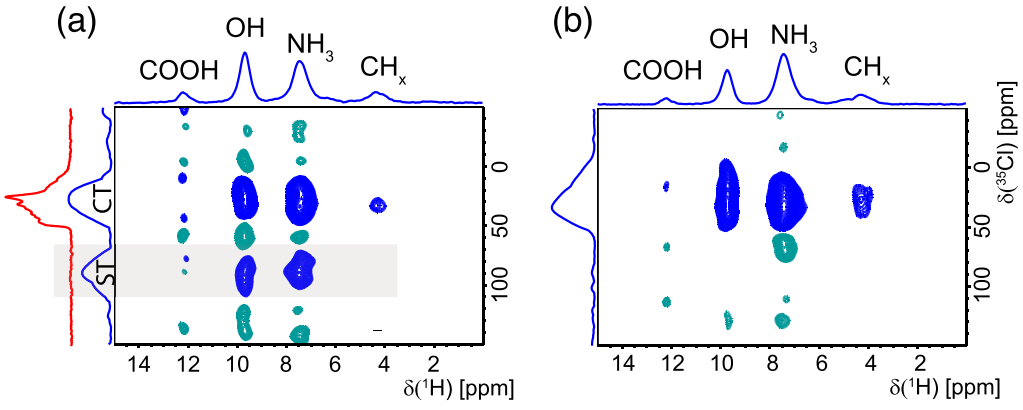

FIGURE 2 (a) ^{35}Cl–^{1}H (850 MHz) dipolar heteronuclear multiple-quantum coherence (D-HMQC) magic-angle spinning (MAS) (60 kHz) nuclear magnetic resonance (NMR) spectra with skyline projections of L-tyrosine·HCl recorded with $\tau^1_{RCPL} = \tau^2_{RCPL} = 400$ μs of $SR4^2_1$ heteronuclear recoupling (a) without or (b) with WURST saturation of the ^{35}Cl satellite transitions (see pulse sequence diagrams in Figure 1). One hundred twenty-eight transients were co-added for each of 100 rotor-synchronised t_1 free-induction decays (FIDs) with a 1 s recycle delay, corresponding to a total experimental time of 4 h. Positive and negative contours are shown in blue and green, respectively, with the base contour level at (a) 15% and (b) 12% of the maximum peak intensity. The furthest left vertical projection shows a spin-echo ^{35}Cl MAS NMR spectrum. A two-dimensional (2D) spectrum obtained with phase-inverted R^3 recoupling is shown in Figure S1

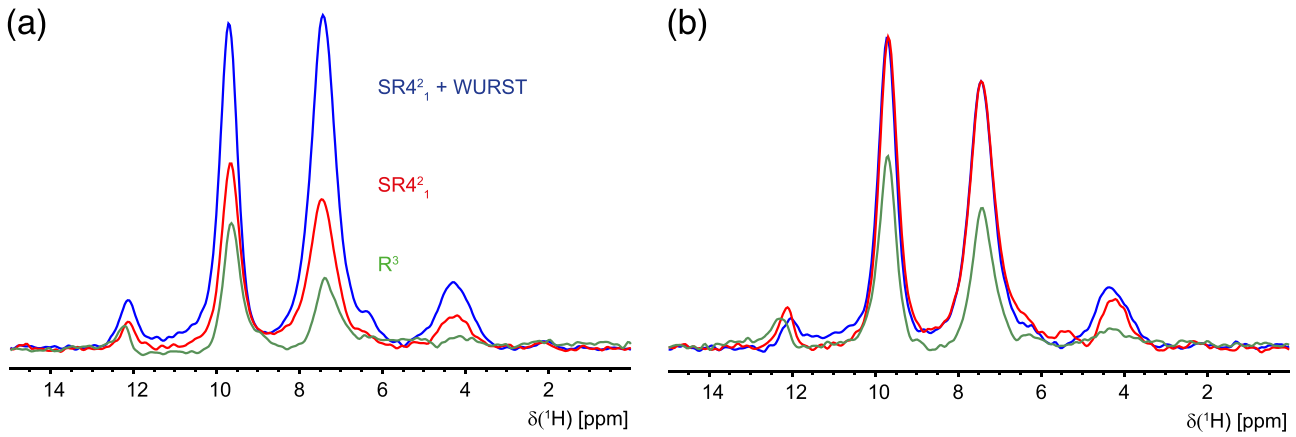

FIGURE 3 A comparison of summed rows from ^{35}Cl–^{1}H (850 MHz) dipolar heteronuclear multiple-quantum coherence (D-HMQC) ($\tau^1_{RCPL} = \tau^2_{RCPL} = 400$ μs) magic-angle spinning (MAS) (60 kHz) nuclear magnetic resonance (NMR) spectra of L-tyrosine·HCl recorded with phase-inverted R^3 (green) or $SR4^2_1$ recoupling (pulse sequence in Figure 1a) (red) and with $SR4^2_1$ recoupling and WURST saturation of the ^{35}Cl satellite transitions (pulse sequence in Figure 1b) (blue). The sum of the F_2 ^{1}H spectra over the ^{35}Cl F_1 dimension is (a) from −20 to 60 ppm corresponding to the ^{35}Cl central transition and (b) from −20 to 120 ppm corresponding to the ^{35}Cl (a) central transition and (b) satellite transitions. The ^{1}H and the ^{35}Cl transmitter frequencies were set to 8.7 and 24 ppm, respectively

FIGURE 4 The dependence of signal intensity upon the recoupling time, $\tau_{RCPL} = \tau^1_{RCPL} = \tau^2_{RCPL}$, in ^{35}Cl–^{1}H (850 MHz) population transfer dipolar heteronuclear multiple-quantum coherence (PT-D-HMQC) magic-angle spinning (MAS) (60 kHz) nuclear magnetic resonance (NMR) spectra. (a) Experimental results for L-tyrosine·HCl recorded using the pulse sequence shown in Figure 1b with $SR4^2_1$ recoupling and WURST saturation of the ^{35}Cl satellite transitions. Sum (over the ^{35}Cl dimension) of the ^{1}H spectral region from 1.0 to 11.2 ppm of the 2D correlation spectra is displayed, with the OH and NH_3^+ resonances at 9.7 and 7.3 ppm, respectively. (b) Simulated (SIMPSON) intensity of the recoupling in the ^{35}Cl–^{1}H D-HMQC experiment for one ^{35}Cl (with $C_Q = 2.4$ MHz and $\eta = 0.72$) and one ^{1}H, starting from I_x coherence and monitoring evolution of the I_yS_z term, for a dipolar coupling (collinear principal axes systems, PASs) of 1.2 (circles), 1.0 (triangles) and 0.8 kHz (squares), corresponding to a Cl–H distance of 2.14, 2.27 and 2.45 Å, respectively

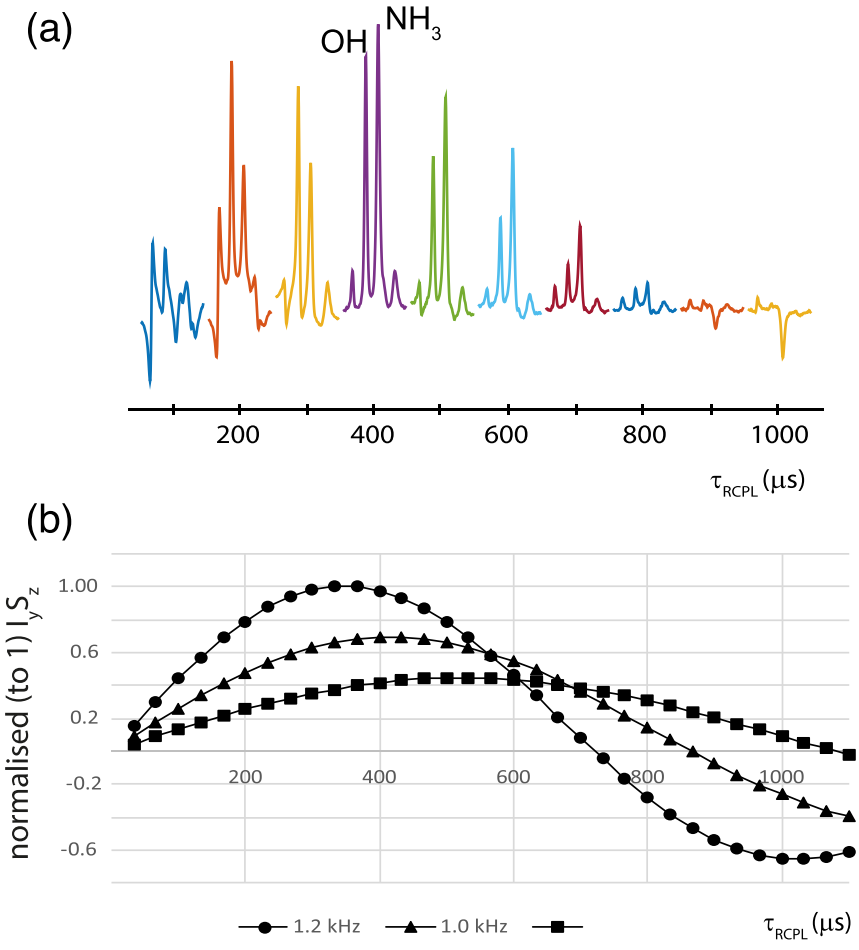

the τ^1_{RCPL} and τ^2_{RCPL} recoupling durations are increased from 100 μs to 1 ms. For both the NH_3^+ ^{1}H resonance at 7.3 ppm and the OH ^{1}H resonance at 9.7 ppm, a clear maximum is observed at 400 μs (24 rotor periods). The experimental results when either τ^1_{RCPL} or τ^2_{RCPL} is increased independently are shown in Figure S2. In this

case, evolution under the ^{1}H CSA distorts the recoupling build-up profile.

It is informative to compare the experimental results to simulations for a ^{35}Cl–^{1}H 2-spin system undergoing SR4$^{2}_{1}$ recoupling using the SIMPSON simulation package.[60] The PT-D-HMQC experiment aims to excite and detect the double quantum (DQ) coherence term between ^{1}H and ^{35}Cl spins; therefore, the spin dynamics of the PT-D-HMQC experiment can be described using product operator formalism in a similar way as presented by Mandal et al.[61] Therefore, we used the SIMPSON programme (code shown in the Supporting Information, Section S6) to calculate the evolution of the I_yS_z term under the R4$^{2}_{1}$ recoupling sequence when starting with I_x.

Simulated build-up for a dipolar coupling of 1.2, 1, and 0.8 kHz (corresponding to a Cl–H distance of 2.14, 2.27 and 2.45 Å, respectively) are shown in Figure 4b. Comparing the shape of the experimental build-up in Figure 4a for the L-tyrosine HCl OH ^{1}H resonance to the simulated build-up curves, there is good agreement for the initial build-up of the 1.2 kHz (2.1 Å) simulated data with the experimental data for the OH peak, whereas the experimental data for the NH_3 peak have maximum intensity that best matches the simulated data for 1.0 kHz. In this respect, for the crystal structure (CSD code LTYRHC10[62]), after density functional theory (DFT) (CASTEP) geometry optimization, the closest Cl–H (OH group) distance is 2.08 Å. For the NH_3^+ group, the Cl–H distances are 2.3, 2.4 and 2.5 Å; considering also the NH_3^+ group rotation, it is informative that there is a good match between the experimental data in Figure 4 and the simulated two-spin build-up curve for a distance of 2.27 Å.

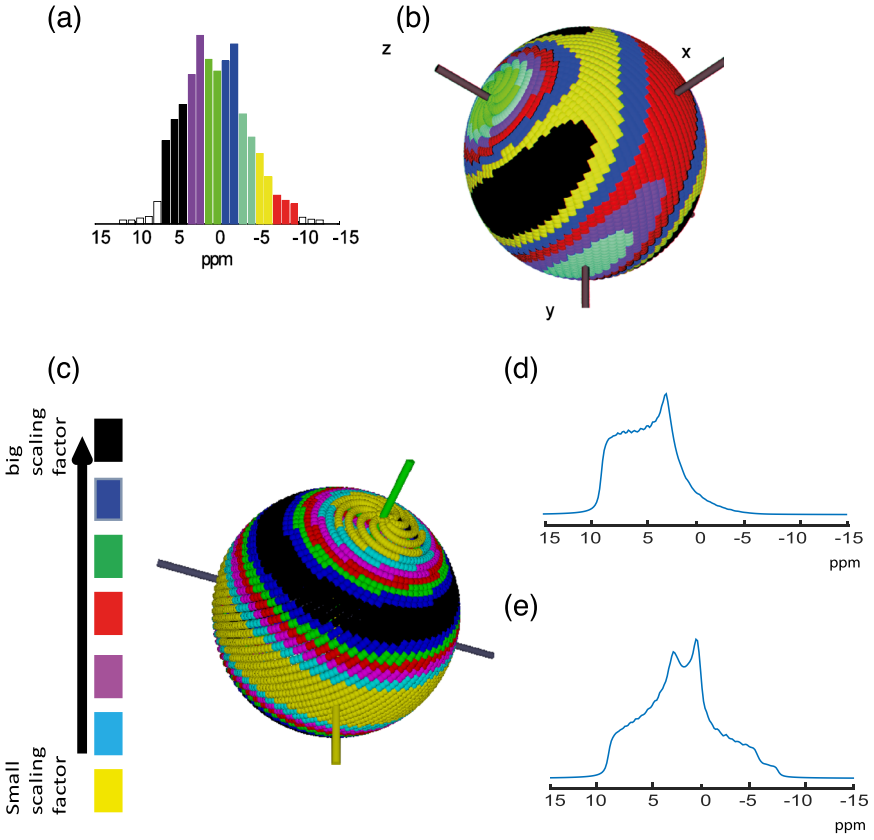

FIGURE 5 An investigation using the SIMPSON software of how different orientations contribute to the second-order quadrupolar nuclear magnetic resonance (NMR) powder-pattern lineshape under magic-angle spinning (MAS) (60 kHz) for a ^{35}Cl nucleus with $C_Q = 2.4$ MHz and $\eta = 0.72$. (a) a histogram representation, whereby each orientation of the SIMPSON ZCW6044 crystal file has been considered independently such that the height of each bar represents the number of orientations which resonate in that frequency interval. (b) Different colours are used to identify the orientations that contribute to different frequency intervals of the lineshape in (a). (c) Colour-coded distribution of the scaling factor for all orientations in a powder of ^{35}Cl nuclei coupled to a ^{1}H nucleus, with a dipolar coupling of 1 kHz and collinear principal axes systems (PASs), with the dipolar tensor having the same orientation as the quadrupolar tensor (for the case that the quadrupolar and dipolar tensors have different orientations, see Figure S5) for 266.67 μs of ^{35}Cl–^{1}H SR4$^{2}_{1}$ recoupling. The starting operator is I_x and the detect operator is I_yS_z. (d, e) simulated lineshapes of the ^{35}Cl central transition if different orientations of the quadrupolar tensor are (d) excited according to the scaling factors shown on (c) or (e) if different orientations of the quadrupolar tensor are evenly excited (undistorted lineshape). Simulations correspond to a ^{1}H Larmor frequency of 850 MHz

When τ^1_{RCPL} is equal to τ^2_{RCPL}, the ^{1}H CSA is refocused by the 180° pulse. However, when this is not the case, the ^{1}H CSA has a strong influence on the recoupling sequence as shown experimentally (compare Figures 4a and S2) and in the simulations in Figure S3.

The simulations in Figure 4b are for a powder average. However, it must be remembered that different orientations in the powder, corresponding (when averaged over a rotor period for MAS) to different parts of the second-order quadrupolar-broadened lineshape, experience different quadrupolar interaction magnitudes and have a different relative orientation of the quadrupolar tensor with respect to the ^{35}Cl–^{1}H internuclear vector (corresponding to the principal axis of the dipolar coupling) so that they will be affected differently by the recoupling sequence. Therefore, we performed numerical simulation of the intensity of ^{35}Cl–^{1}H D-HMQC experiment individually for each orientation of the ^{35}Cl quadrupolar tensor in a powder distribution. This reveals a strong dependence of the heteronuclear dipolar recoupling on the orientation of the quadrupolar tensor as is shown in Figure 5c. Similar symmetry of the scaling factor has been obtained for phase-inverted R^3 recoupling (see Figure S5a). Such an investigation into the contributions from different orientations is useful in providing an insight into the experimental observations, specifically when looking at how different regions of the quadrupolar lineshape are affected by the recoupling. Figures 5a,b considers the second-order quadrupolar lineshape for a powder sample with $C_Q = 2.4$ MHz and $\eta = 0.72$. Different colours are used to identify the orientations that contribute to different frequency intervals of the lineshape. Figure 5c shows how the $SR4^2_1$ recoupling is distributed over all the orientations in a powder with regions displayed in black being preferentially recoupled, whereas the orientations displayed in yellow experience a weak recoupling to a ^{1}H nucleus. Quantifying the change in intensity upon recoupling for each orientation that contributes to the second-order quadrupolar lineshape results in a distorted spectrum as shown in Figure 5d for 266.67 μs of $SR4^2_1$ recoupling. Figure S4 shows corresponding plots for 33.3 or 1,000 μs of $SR4^2_1$ recoupling, whereas Figure S5 considers different relative orientations of the dipolar and quadrupolar tensors.

3.3 | ^{1}H and ^{35}Cl MAS NMR one-dimensional spectra and GIPAW calculations for amino acids and pharmaceuticals

This and the following section present MAS NMR spectra for two amino acids, glycine·HCl as well as L-tyrosine HCl, and three pharmaceuticals, amitriptyline·HCl,

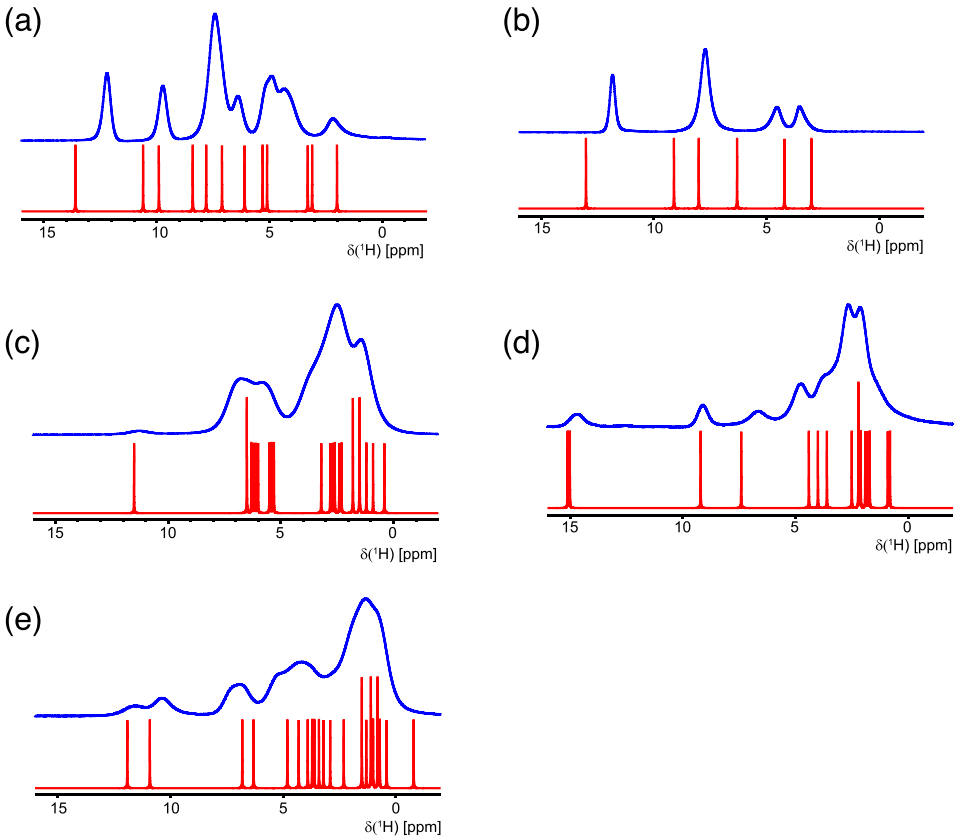

FIGURE 6 ^{1}H (850 MHz) magic-angle spinning (MAS) (60 kHz) nuclear magnetic resonance (NMR) single-pulse spectra with background suppression[50] (top, in blue) together with stick-spectra (bottom, in red) representations of the gauge-including projector-augmented wave (GIPAW)-calculated ^{1}H chemical shifts for (a) L-tyrosine·HCl, (b) glycine·HCl, (c) amitriptyline·HCl, (d) cimetidine·HCl and (e) lidocaine·HCl·H_2O. Sixteen transients were co-added for a 2-s recycle delay, corresponding to a total experimental time of 32 s

cimetidine·HCl and lidocaine·HCl·H_2O (see chemical structures in Figures S7–S11). Specifically, this section presents one-dimensional ^{1}H and ^{35}Cl MAS NMR spectra in Figures 6 and 7, respectively. GIPAW calculations of the ^{1}H and ^{35}Cl chemical shift and ^{35}Cl quadrupolar parameters (the quadrupolar coupling constant, C_Q, the asymmetry parameter, η_Q, and, hence, the quadrupolar product, P_Q) have been performed in

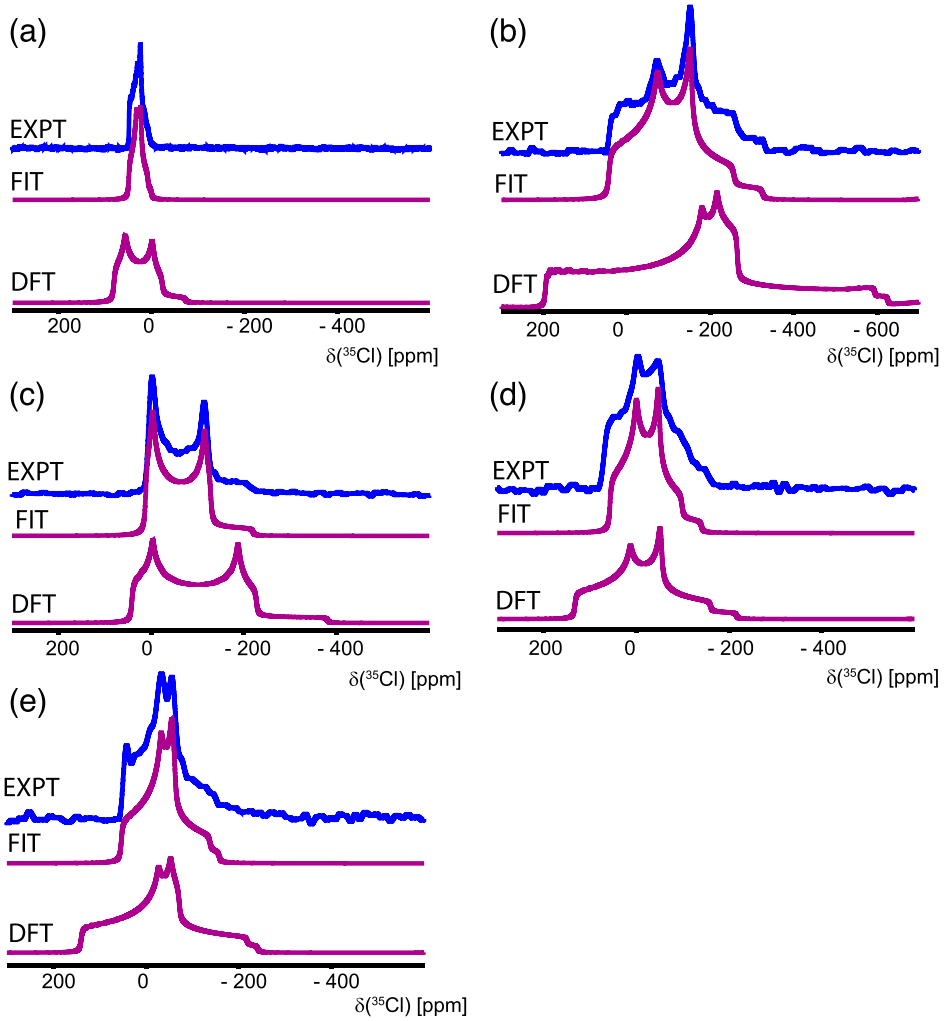

FIGURE 7 WURST enhanced ^{35}Cl (20.0 tesla) spin-echo magic-angle spinning (MAS) nuclear magnetic resonance (NMR) (60 kHz) spectra (2 and 4 μs and 90° and 180° pulses, respectively, with a 2-rotor period echo duration; top, in blue), together with simulated (SIMPSON) second-order quadrupolar-broadened lineshapes (upper: Best-by-eye fit to the experimental data; lower for the density functional theory (DFT) (CASTEP) calculated quadrupolar parameters), for (a) L-tyrosine·HCl, (b) glycine·HCl, (c) amitriptyline·HCl, (d) cimetidine·HCl, (e) lidocaine·HCl·H_2O. 10,000, 20,000, 44,000, 40,000 and 40,000 transients were co-added for a 0.2-s recycle delay corresponding to a total experimental time of 0.6, 1.2, 2.4, 2.2 and 2.2 h, respectively

TABLE 1 Experimental and gauge-including projector-augmented wave (GIPAW)-calculated ^{35}Cl nuclear magnetic resonance (NMR) parameters

			Calculated				Experimental[c]			
Compound	CSD code	Ref.	C_Q/MHz	η_Q	P_Q/MHz[a]	δ_{ISO}/ppm[b]	C_Q/MHz	η_Q	P_Q/MHz[a]	δ_{ISO}/ppm
L-Tyrosine·HCl	LTYRHC10	Frey et al.[62]	4.29	0.26	4.34	51.0	2.3	0.8	2.5	51
Glycine·HCl	GLYHCL01	di Blasioet al.[70]	8.96	0.91	10.12	50.8	6.3	0.6	6.6	51
Cimetidine·HCl	EHIWEZ	Watss et al.[63]	6.09	0.63	6.48	63.6	4.7	0.6	4.9	64
Amitriptyline·HCl	YOVZEO	Klein et al.[71]	7.19	0.17	7.22	24.5	5.4	0.1	5.4	44
Lidocaine·HCl·H_2O	LIDOCN01	Hamaed et al.[16]	6.15	0.86	6.87	53.7	4.6	0.8	5.1	56

[a] $P_Q = C_Q\left(1+\frac{\eta_Q^2}{3}\right)^{1/2}$.
[b] The reference shielding is 962 ppm.
[c] The error on the experimental values are ±0.4 MHz for C_Q and P_Q, ±0.2 for η_Q and ±3 ppm for δ_{iso}.

CASTEP for geometry-optimised crystal structures (see Table 1). For ^{1}H, the GIPAW-calculated chemical shifts are presented as stick spectra in Figure 6, with the experimental and GIPAW-calculated values tabulated in Tables S1–S5. GIPAW calculations for L-tyrosine·HCl and glycine·HCl and on cimetidine·HCl have been previously reported.[15,63,64] ^{1}H MAS NMR spectra of cimetidine·HCl have been previously presented in Maruyoshi et al.[65]

When considering ^{35}Cl chemical shifts, it is important to consider the choice of reference. In this work we follow Bryce et al.[13] and use NaCl 0.1-M aqueous solution. To convert to a chemical shift scale where the ^{35}Cl chemical shift of solid NaCl is set to 0 ppm, as for example used by Gervais et al.,[15] it is necessary to add 46 ppm (Eq. 6 in Bryce et al.[13]). It is observed from Figure 7 and Table 1 that the GIPAW-calculated ^{35}Cl C_Q values are a factor of 1.3–1.9 times larger than that determined experimentally. Such a discrepancy has been noted previously[15,64,66,67]; in this context, Socha et al. have shown that better agreement is found for calculations performed using hybrid and meta-generalised gradient approximation (GGA) functionals.[64] Moreover, Holmes et al.[68,69] have used a large training set of organic solids for the parameterization of a DFT dispersion correction so as to achieve better agreement between experimental and calculated electric field gradient tensors.

3.4 | ^{35}Cl–^{1}H PT-D-HMQC MAS NMR spectra for amino acids and pharmaceuticals

Figure 8 presents ^{35}Cl–^{1}H PT-D-HMQC MAS NMR spectra recorded at a ^{1}H Larmor frequency of 850 MHz and a MAS frequency of 60 kHz for (a) glycine·HCl, (b) amitriptyline·HCl, (c) cimetidine·HCl and (d) lidocaine·HCl·H_2O. For comparison, as well as skyline projections (in blue), one-dimensional ^{1}H one-pulse (top, in red) and ^{35}Cl echo (left, in green) MAS NMR spectra are also shown. The observed ^{35}Cl–^{1}H correlation

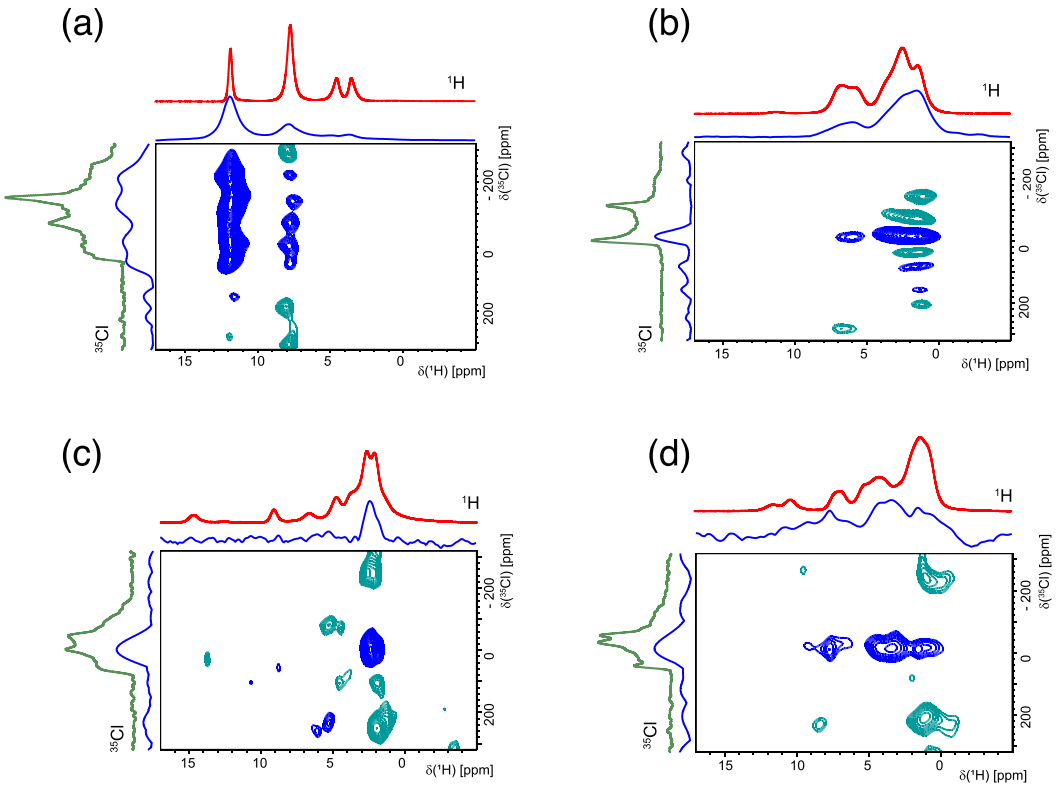

FIGURE 8 ^{35}Cl–^{1}H (850 MHz) population transfer dipolar heteronuclear multiple-quantum coherence (PT-D-HMQC) magic-angle spinning (MAS) (60 kHz) nuclear magnetic resonance (NMR) spectra, together with skyline projections (in blue) and one-dimensional ^{1}H one-pulse (top, in red) and ^{35}Cl echo (left, in green) MAS NMR spectra, recorded with $\tau^{1}_{RCPL} = \tau^{2}_{RCPL} = 400$ μs of $SR4^{2}_{1}$ heteronuclear recoupling with WURST saturation of the ^{35}Cl satellite transitions (see pulse sequence diagram in Figure 1b), of (a) glycine·HCl, (b) amitriptyline·HCl, (c) cimetidine·HCl and (d) lidocaine·HCl·H_2O. The ^{1}H and the ^{35}Cl transmitter frequencies were set to 10.9 and 40 ppm, respectively, for all four experiments. (a) 2,000, (b) 4,000, (c) 4,000 and (d) 1,600 transients were co-added for each of (a) 24, (b) 40, (c) 16 and (d) 30 rotor-synchronised t_1 FIDs with a recycle delay of 1 s, corresponding to an experimental time of (a) 14, (b) 22, (c) 22 and (d) 13 h. The base contour levels are at (a) 12.5%, (b) 25%, (c) 25% and (d) 50% of the maximum peak intensity

peaks correspond to the closest H–Cl distances as revealed by the (CASTEP geometry optimised) crystal structures. For glycine·HCl (Figure 8a), cross peaks are observed with the amine and the carboxylic acid protons, at 7.7 and 11.8 ppm, respectively, for which the closest H–Cl distances (see Figure S8 and Table S2) to the chloride ion are at 1.9 and 2.1 Å, respectively. Note that the quadrupolar product, P_Q, is biggest of all the samples studied in this paper (6.6 MHz, see Table 1), as evident from the greater extent of second-order quadrupolar broadening of the ^{35}Cl lineshape.

For amytriptiline·HCl (Figure 8b), the crystal structure (see Figure S9 and Table S3) indicates that a NH proton H93 at 11.3 ppm, a CH_2 proton H65 at 2.6 ppm and a CH_3 proton H89 at 2.8 ppm are closest to the chloride ion at 1.9, 2.7 and 2.7 Å, respectively. For cimetidine·HCl (Figure 8c), the crystal structure (see Figure S10 and Table S4) shows that the NH protons H1 at 15.0 ppm and H9 at 15.1 ppm, the imidazole H5 at 9.1 ppm and the CH_2 H33 at 4.0 ppm are at 2.0, 2.0, 2.6 and 2.8 Å away from the chloride ion, respectively. For lidocaine·HCl·H_2O (Figure 8d), the crystal structure (see Figure S11 and Table S5) indicates the NH proton H89 at 11.9 ppm, the H_2O H97 at 4.3 ppm and the CH_3 H81 at 1.3 ppm are at 2.0, 2.2 and 2.9 Å, respectively away from ^{35}Cl. In each of Figure 8b–d, while Cl–H cross peaks are observed at lower ppm ^{1}H resonances, corresponding to the most intense alkyl ^{1}H peaks in the one-pulse spectra in Figure 6, disappointingly no peaks are evident for the low-intensity high-ppm NH resonances. Especially for Figure 6b–d where the ^{1}H MAS intensity of the OH and NH moieties is considerably lower compared with the aliphatic ^{1}H signal, a considerable boost in sensitivity of the PT-D-HMQC is required for the ^{35}Cl–^{1}H correlation for the OH and NH sites to become visible.

4 | CONCLUSIONS AND OUTLOOK

This paper presents applications of a ^{35}Cl–^{1}H D-HMQC MAS NMR experiment incorporating WURST saturation of the ^{35}Cl satellite transitions in a PT-D-HMQC approach to probe and identify proximity between chloride ions and protons in amino acids and pharmaceutical HCl salts. Density-matrix numerical simulation (using SIMPSON) of the effect of orientation of the quadrupolar tensor on the recoupling performance shows a strong anisotropic dependence that distorts the quadrupolar lineshape. For L-tyrosine·HCl, the distance between ^{1}H and ^{35}Cl atoms can be quantified by recording D-HMQC build-up curves, as recorded by incrementing the recoupling time. DFT calculations using the CASTEP GIPAW code gives calculated ^{35}Cl quadrupolar coupling constants larger than those determined by experiment as observed by others.

The PT-D-HMQC MAS NMR spectra presented in this paper often suffer from marked t_1 noise due to the strong dependence of the recoupling Hamiltonian rotor phase on small fluctuations in the MAS frequency. In this respect, we note that various approaches to reduce t_1 noise, for example, based on using pi pulses to remove the CSA evolution during recoupling, have been introduced.[59,72,73] A ^{35}Cl–^{1}H DQ HMQC experiment, recently introduced by Hung et al.,[74] provides higher resolution for ^{35}Cl by reducing the second-order quadrupolar broadening for a DQ coherence corresponding to the sum of the central transition and the satellite transition for the spin-3/2 ^{35}Cl nucleus. Also, it may be convenient to exploit the shorter T_1 of the quadrupolar nucleus and perform X detected X—^{1}H D-INEPT experiments as has been demonstrated by Venkatesh et al.[31] for ^{35}Cl, ^{71}Ga and ^{27}Al. There is thus much potential for the further development of ^{35}Cl–^{1}H heteronuclear correlation MAS NMR experiments.

ACKNOWLEDGEMENTS

The UK 850-MHz Solid-State NMR Facility used in this research was funded by the Engineering and Physical Sciences Research Council (EPSRC) and the Biotechnology and Biological Sciences Research Council (BBSRC) (PR140003 and EP/T015063/1), as well as the University of Warwick including via part funding through Birmingham Science City Advanced Materials Projects 1 and 2 supported by Advantage West Midlands (AWM) and the European Regional Development Fund (ERDF). We thank Sarah Mann, Azzedine Dabo and Jozef Lewandowski for providing the Lidocaine and Amitriptyline samples. Emily Corlett thanks EPSRC, AstraZeneca and Syngenta for a PhD studentship through the EPSRC Centre for Doctoral Training in Molecular Analytical Science, grant number EP/L015307/1. The calculated and experimental data for this study are provided as a supporting data set from WRAP, the Warwick Research Archive Portal at http://wrap.warwick.ac.uk/155058.

PEER REVIEW

The peer review history for this article is available at https://publons.com/publon/10.1002/mrc.5188.

ORCID

Dinu Iuga https://orcid.org/0000-0001-9315-8250
Steven P. Brown https://orcid.org/0000-0003-2069-8496

REFERENCES

[1] M. N. Anurova, E. O. Bakhrushina, N. B. Demina, E. S. Panteleeva, *Pharm. Chem. J.* **2019**, *53*, 564.

[2] R. V. Moiseev, P. W. J. Morrison, F. Steele, V. V. Khutoryanskiy, *Pharmaceutics* **2019**, *11*, 321.

[3] G. S. Paulekuhn, J. B. Dressman, C. Saal, *J. Med. Chem.* **2007**, *50*, 6665.

[4] A. C. Mafud, E. W. Reinheimer, F. C. D. A. Lima, L. F. Batista, K. de Paula, L. M. C. Véras, J. R. de Souza de Almeida Leite, T. Venancio, Y. P. Mascarenhas, *J. Mol. Struct.* **2017**, *1136*, 204.

[5] A. M. Namespetra, D. A. Hirsh, M. P. Hildebrand, A. R. Sandre, H. Hamaed, J. M. Rawson, R. W. Schurko, *CrystEngComm* **2016**, *18*, 6213.

[6] S. P. Brown, *Solid State Nucl. Magn. Reson.* **2012**, *41*, 1.

[7] D. A. Hirsh, A. J. Rossini, L. Emsley, R. W. Schurko, *Phys. Chem. Chem. Phys.* **2016**, *18*, 25893.

[8] M. Hildebrand, H. Hamaed, A. M. Namespetra, J. M. Donohue, R. Fu, I. Hung, Z. Gan, R. W. Schurko, *CrystEngComm* **2014**, *16*, 7334.

[9] C. M. Widdifield, R. P. Chapman, D. L. Bryce, *Annu. Rep. NMR Spectrosc.* **2009**, *66*, 195.

[10] R. P. Chapman, C. M. Widdifield, D. L. Bryce, *Prog. Nucl. Magn. Reson. Spectrosc.* **2009**, *55*, 215.

[11] P. M. J. Szell, D. L. Bryce, *Annu. Rep. NMR Spectrosc.* **2015**, *84*, 115.

[12] F. A. Perras, D. L. Bryce, *Angew. Chem.-Int. Edit.* **2012**, *51*, 4227.

[13] D. L. Bryce, M. Gee, R. E. Wasylishen, *J. Phys. Chem. A* **2001**, *105*, 10413.

[14] R. P. Chapman, D. L. Bryce, *Phys. Chem. Chem. Phys.* **2007**, *9*, 6219.

[15] C. Gervais, R. Dupree, K. J. Pike, C. Bonhomme, M. Profeta, C. J. Pickard, F. Mauri, *J. Phys. Chem. A* **2005**, *109*, 6960.

[16] H. Hamaed, J. M. Pawlowski, B. F. Cooper, R. Fu, S. H. Eichhorn, R. W. Schurko, *J. Am. Chem. Soc.* **2008**, *130*, 11056.

[17] F. G. Vogt, G. R. Williams, M. Strohmeier, M. N. Johnson, R. C. B. Copley, *J. Phys. Chem. B* **2014**, *118*, 10266.

[18] D. L. Bryce, G. D. Sward, *J. Phys. Chem. B* **2006**, *110*, 26461.

[19] Z. Yao, H.-T. Kwak, D. Sakellariou, L. Emsley, P. J. Grandinetti, *Chem. Phys. Lett.* **2000**, *327*, 85.

[20] D. Iuga, A. P. M. Kentgens, *J. Magn. Reson.* **2002**, *158*, 65.

[21] R. Siegel, T. T. Nakashima, R. E. Wasylishen, *Chem. Phys. Lett.* **2004**, *388*, 441.

[22] K. K. Dey, S. Prasad, J. T. Ash, M. Deschamps, P. J. Grandinetti, *J. Magn. Reson.* **2007**, *185*, 326.

[23] L. A. O'Dell, *Solid State Nucl. Magn. Reson.* **2013**, *55-56*, 28.

[24] R. Siegel, T. T. Nakashima, R. E. Wasylishen, *J. Magn. Reson.* **2007**, *184*, 85.

[25] M. Goswami, P. J. M. van Bentum, A. P. M. Kentgens, *J. Magn. Reson.* **2012**, *219*, 25.

[26] M. Goswami, P. J. M. van Bentum, A. P. M. Kentgens, *Can. J. Chem.* **2011**, *89*, 1130.

[27] Q. Wang, J. Trébosc, Y. Li, O. Lafon, S. Xin, J. Xu, B. Hu, N. Feng, J.-P. Amoureux, F. Deng, *J. Magn. Reson.* **2018**, *293*, 92.

[28] D. Iuga, P. Rossi, J. Herzfeld, R. G. Griffin, *Solid State Nucl. Magn. Reson.* **2017**, *82-83*, 35.

[29] A. S. Tatton, J. P. Bradley, D. Iuga, S. P. Brown, *Z. Phys. Chem.* **2012**, *226*, 1187.

[30] M. K. Pandey, H. Kato, Y. Ishii, Y. Nishiyama, *Phys. Chem. Chem. Phys.* **2016**, *18*, 6209.

[31] A. Venkatesh, M. P. Hanrahan, A. J. Rossini, *Solid State Nucl. Magn. Reson.* **2017**, *84*, 171.

[32] D. A. Hirsh, A. V. Wijesekara, S. L. Carnahan, I. Hung, J. W. Lubach, K. Nagapudi, A. J. Rossini, *Mol. Pharmaceutics* **2019**, *16*, 3121.

[33] T. G. Oas, R. G. Griffin, M. H. Levitt, *J. Chem. Phys.* **1988**, *89*, 692.

[34] P. R. Costa, J. D. Gross, M. Hong, R. G. Griffin, *Chem. Phys. Lett.* **1997**, *280*, 95.

[35] M. Carravetta, M. Edén, X. Zhao, A. Brinkmann, M. H. Levitt, *Chem. Phys. Lett.* **2000**, *321*, 205.

[36] A. Brinkmann, A. P. M. Kentgens, *J. Am. Chem. Soc.* **2006**, *128*, 14758.

[37] X. Lu, O. Lafon, J. Trebosc, G. Tricot, L. Delevoye, F. Mear, L. Montagne, J. P. Amoureux, *J. Chem. Phys.* **2012**, *137*, 144201.

[38] Z. Gan, J. P. Amoureux, J. Trébosc, *Chem. Phys. Lett.* **2007**, *435*, 163.

[39] S. Cavadini, S. Antonijevic, A. Lupulescu, G. Bodenhausen, *J. Magn. Reson.* **2006**, *182*, 168.

[40] Y. Nishiyama, Y. Endo, T. Nemoto, H. Utsumi, K. Yamauchi, K. Hioka, T. Asakura, *J. Magn. Reson.* **2011**, *208*, 44.

[41] K. Maruyoshi, D. Iuga, O. N. Antzutkin, A. Alhalaweh, S. P. Velaga, S. P. Brown, *Chem. Commun.* **2012**, *48*, 10844.

[42] A. S. Tatton, T. N. Pham, F. G. Vogt, D. Iuga, A. J. Edwards, S. P. Brown, *Mol. Pharmaceutics* **2013**, *10*, 999.

[43] A. S. Tatton, T. N. Pham, F. G. Vogt, D. Iuga, A. J. Edwards, S. P. Brown, *CrystEngComm* **2012**, *14*, 2654.

[44] Q. Wang, Y. Li, J. Trébosc, O. Lafon, J. Xu, B. Hu, N. Feng, Q. Chen, J.-P. Amoureux, F. Deng, *J. Chem. Phys.* **2015**, *142*, 094201.

[45] Q. Wang, J. Trébosc, Y. Li, J. Xu, B. Hu, N. Feng, Q. Chen, O. Lafon, J.-P. Amoureux, F. Deng, *Chem. Commun.* **2013**, *49*, 6653.

[46] N. T. Duong, F. Rossi, M. Makrinich, A. Goldbourt, M. R. Chierotti, R. Gobetto, Y. Nishiyama, *J. Magn. Reson.* **2019**, *308*, 106559.

[47] A. V. Wijesekara, A. Venkatesh, B. J. Lampkin, B. VanVeller, J. W. Lubach, K. Nagapudi, I. Hung, P. L. Gor'kov, Z. Gan, A. J. Rossini, *Chem. – Eur. J.* **2020**, *26*, 7881.

[48] R. K. Harris, E. D. Becker, S. M. C. de Menezes, P. Granger, R. E. Hoffman, K. W. Zilm, *Magn. Reson. Chem.* **2008**, *46*, 582.

[49] S. Hayashi, K. Hayamizu, *Bull. Chem. Soc. Jpn.* **1991**, *64*, 685.

[50] D. G. Cory, W. M. Ritchey, *Spectrosc. Lett.* **1988**, *21*, 551.

[51] A. L. Webber, S. Masiero, S. Pieraccini, J. C. Burey, A. S. Tatton, D. Iuga, T. N. Pham, G. P. Spada, S. P. Brown, *J. Am. Chem. Soc.* **2011**, *133*, 19777.

[52] S. J. Huang, S. B. Liu, J. C. C. Chan, *Solid State Nucl. Magn. Reson.* **2009**, *36*, 110.

[53] E. Kupce, R. Freeman, *J. Magn. Reson. Ser. A* **1995**, *115*, 273.

[54] Ē. Kupce, R. Freeman, *J. Magn. Reson. Ser. A* **1996**, *118*, 299.

[55] D. J. States, R. A. Haberkorn, D. J. Ruben, *J. Magn. Reson.* **1982**, *48*, 286.

[56] S. J. Clark, M. D. Segall, C. J. Pickard, P. J. Hasnip, M. I. J. Probert, K. Refson, M. C. Payne, *Z. Kristallogr. Cryst. Mater.* **2005**, *220*, 567.

[57] J. P. Perdew, K. Burke, M. Ernzerhof, *Phys. Rev. Lett.* **1996**, *77*, 3865.

[58] C. J. Pickard, F. Mauri, *Phys. Rev. B* **2001**, *63*, 245101.

[59] A. Venkatesh, X. Luan, F. A. Perras, I. Hung, W. Huang, A. J. Rossini, *Phys. Chem. Chem. Phys.* **2020**, *22*, 20815.

[60] M. Bak, J. T. Rasmussen, N. C. Nielsen, *J. Magn. Reson.* **2000**, *147*, 296.
[61] P. K. Mandal, A. Majumdar, *Concept Magn. Reson. Part A* **2004**, *20A*, 1.
[62] M. N. Frey, T. F. Koetzle, M. S. Lehmann, W. C. Hamilton, *J. Chem. Phys.* **1973**, *58*, 2547.
[63] A. E. Watts, K. Maruyoshi, C. E. Hughes, S. P. Brown, K. D. M. Harris, *Cryst. Growth des.* **2016**, *16*, 1798.
[64] O. Socha, P. Hodgkinson, C. M. Widdifield, J. R. Yates, M. Dracinsky, *J. Phys. Chem. A* **2017**, *121*, 4103.
[65] K. Maruyoshi, D. Iuga, A. E. Watts, C. E. Hughes, K. D. M. Harris, S. P. Brown, *J. Pharm. Sci.* **2017**, *106*, 3372.
[66] D. L. Bryce, E. B. Bultz, *Chem.-Eur. J.* **2007**, *13*, 4786.
[67] R. P. Chapman, J. R. Hiscock, P. A. Gale, D. L. Bryce, *Can. J. Chem.-Rev. Can. Chim.* **2011**, *89*, 822.
[68] S. T. Holmes, R. W. Schurko, *J. Phys. Chem. C* **2018**, *122*, 1809.
[69] S. T. Holmes, C. S. Vojvodin, R. W. Schurko, *J. Phys. Chem. A* **2020**, *124*, 10312.
[70] B. di Blasio, V. Pavone, C. Pedone, *Cryst. Struct. Commun.* **1977**, *6*, 745.
[71] C. L. Klein, J. Lear, S. O'Rourke, S. Williams, L. Liang, *J. Pharm. Sci.* **1994**, *83*, 1253.
[72] R. Giovine, J. Trébosc, F. Pourpoint, O. Lafon, J.-P. Amoureux, *J. Magn. Reson.* **2019**, *299*, 109.
[73] Y. Nishiyama, V. Agarwal, R. Zhang, *J. Phys. Chem. C* **2020**, *124*, 26332.
[74] I. Hung, Z. Gan, *J. Phys. Chem. Lett.* **2020**, *11*, 4734.

SUPPORTING INFORMATION

Additional supporting information may be found online in the Supporting Information section at the end of this article.

How to cite this article: D. Iuga, E. K. Corlett, S. P. Brown, *Magn Reson Chem* **2021**, 1. https://doi.org/10.1002/mrc.5188